energies

MDPI

Article

CO_2 Capture and Enhanced Hydrogen Production Enabled by Low-Temperature Separation of PSA Tail Gas: A Detailed Exergy Analysis

David Berstad [1,*], Julian Straus [1] and Truls Gundersen [2]

[1] SINTEF Energy Research, 7034 Trondheim, Norway; julian.straus@sintef.no
[2] Department of Energy and Process Engineering, Norwegian University of Science and Technology (NTNU), 7491 Trondheim, Norway; truls.gundersen@ntnu.no
* Correspondence: david.berstad@sintef.no; Tel.: +47-411-44-876

Abstract: Hydrogen from natural gas reforming can be produced efficiently with a high CO_2 capture rate. This can be achieved through oxygen-blown autothermal reforming as the core technology, combined with pressure-swing adsorption for hydrogen purification and refrigeration-based tail gas separation for CO_2 capture and recirculation of residual hydrogen, carbon monoxide, and methane. The low-temperature tail gas separation section is presented in detail. The main objective of the paper is to study and quantify the exergy efficiency of this separation process in detail. To achieve this, a detailed exergy analysis is conducted. The irreversibilities in 42 different process components are quantified. In order to provide transparent verification of the consistency of exergy calculations, the total irreversibility rate is calculated by two independent approaches: Through the bottom-up approach, all individual irreversibilities are added to obtain the total irreversibility rate. Through the top-down approach, the total irreversibility rate is calculated solely by the exergy flows crossing the control volume boundaries. The consistency is verified as the comparison of results obtained by the two methods shows a relative deviation of $4{\cdot}10^{-7}$. The exergy efficiency of the CO_2 capture process is calculated, based on two different definitions. Both methods give a baseline exergy efficiency of 58.38%, which indicates a high degree of exergy utilisation in the process.

Keywords: CO_2 capture; hydrogen; tail gas; separation; exergy

Citation: Berstad, D.; Straus, J.; Gundersen, T. CO_2 Capture and Enhanced Hydrogen Production Enabled by Low-Temperature Separation of PSA Tail Gas: A Detailed Exergy Analysis. *Energies* **2024**, *17*, 1072. https://doi.org/10.3390/en17051072

Academic Editor: Muhammad Aziz

Received: 16 January 2024
Revised: 7 February 2024
Accepted: 17 February 2024
Published: 23 February 2024

1. Background and Motivation

Hydrogen is considered an enabling technology for utilising fossil fuels, such as natural gas and coal with low CO_2 emissions [1]. With respect to CO_2 capture, an important feature of pre-combustion technologies is the advantage of high CO_2 fraction and partial pressure, which enables less energy-demanding CO_2 capture. Whereas direct combustion of fossil fuels generates flue gases with low CO_2 concentrations and partial pressures, fossil fuels can be converted to synthesis gas, in which CO_2 is available in higher concentrations and at partial pressures that can be orders of magnitude higher than in flue gases.

The most proposed CO_2 capture solutions involve the use of chemical solvents in combination with pressure-swing adsorption (PSA) for hydrogen purification. Since they are largely based on existing reformer process structures, they are also once-through processes. To achieve high decarbonisation in a once-through structure, the reforming and water–gas shift reactors must provide extreme conversion ratios of alkanes to CO_2 via CO. Moreover, the CO_2 separation stage must provide an extremely high stand-alone CO_2 capture ratio since residual CO_2 eventually leads to additional carbon emissions. If conventional syngas separation technologies are to be fitted with off-gas recycling to increase the CO_2 capture ratio, a dedicated recycle compressor is required, but is unlikely to be an attractive solution [2].

Chemical solvents, despite being a mature technology, are arguably inefficient energy-wise and can even have negative exergy efficiency in pre-combustion applications [3]. To better exploit the high CO_2 concentrations that reforming processes can provide, an innovative solution was proposed by Straus et al. [4], in which a PSA unit is combined with a low-temperature tail gas separation process for CO_2 capture and recirculation of CO, methane, and hydrogen to the upstream water–gas shift reactors and reformer. This solution can achieve a very high global CO_2 capture ratio and simultaneously very high plant efficiency [4]. The high efficiency can partly be explained by a reduction in the parasitic energy requirement for separating the syngas into hydrogen and CO_2. To demonstrate the potential power requirement and exergy efficiency for low-temperature tail gas separation and CO_2 capture, the present work will provide a detailed process description and a detailed exergy analysis of the CO_2 capture process. Figure 1 illustrates how the calculation procedure is structured to go from the basic mass and energy balance of the process model to quantifying the exergy flows, exergy efficiency, and irreversibility distribution, and finally verifying the correctness of results based on a transparent consistency check. The latter element is important but still absent in the literature. Each step in the procedure and results are described in dedicated sections under the Method, Results, and Discussion sections. The main contributions from this exergy analysis are as follows:

- Quantification of the exergy efficiency of a novel process for CO_2 separation, purification, and compression, unambiguously defined as the ratio between the actual power requirement and the minimum exergy requirement for a reversible process;
- Allocation and quantification of all thermodynamic losses in the process;
- Presentation of a procedure to verify the correctness of the results through a transparent consistency check, where two independent calculations of the total irreversibility are compared.

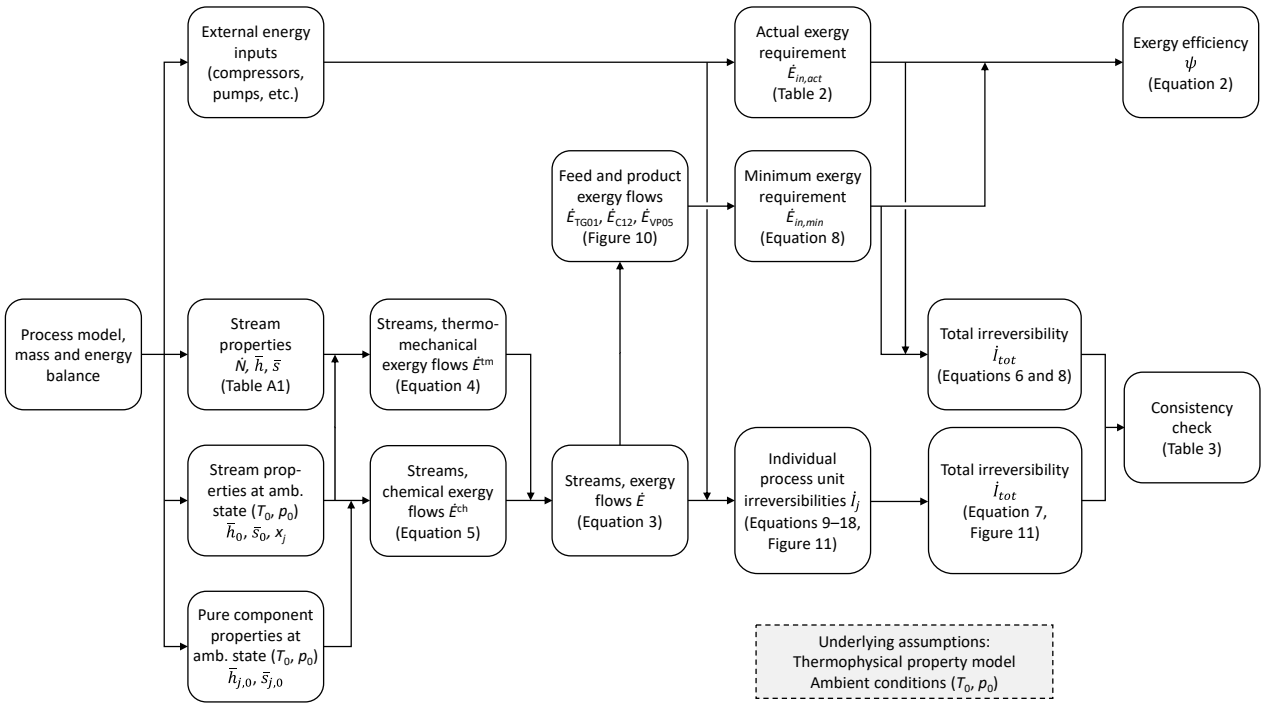

Figure 1. Overview of the calculation procedure for quantifying exergy flows, minimum exergy requirement, irreversibilities, and a transparent consistency check of the results.

The remainder of the paper is organised as follows: Section 2 contains a literature review, Section 3 describes the basics of exergy analysis, including equations for different equipment types, Section 4 describes the overall process for hydrogen production with a more detailed description of the CO_2 capture process, Section 5 presents the results,

Section 6 discusses these results, and Section 7 provides the conclusions that can be drawn from this study.

2. Literature Review

Low-temperature technologies for CO_2 capture through condensation and liquefaction have been studied extensively for several different applications, which will be briefly reviewed in the following.

2.1. Low-Temperature and Cryogenic Post-Combustion CO_2 Capture

Industrial flue gases have far too low CO_2 fractions for the direct liquefaction and separation of CO_2. To achieve phase change and separation of CO_2, direct freeze-out induced by cryogenic temperatures well below the CO_2 solidification temperature is required. Different process structures have been proposed, either for lowering the flue gas stream temperature sufficiently for CO_2 to solidify or for freezing out and depositing CO_2 locally on cold surfaces [5–15].

If a low-temperature technology is combined with a complementary front-end CO_2 enrichment process such as a polymeric membrane, the CO_2 concentrations can become sufficiently high to allow a high fraction of CO_2 to be liquefied in a secondary low-temperature separation stage. Hybrid processes combining CO_2 selective membranes and CO_2 liquefaction have been studied extensively [16–20], where CO_2 processing typically includes vacuum pumping, compression, and partial condensation and separation at temperatures typically at around −50 °C.

2.2. CO_2 Capture from Oxyfuel Combustion

In oxyfuel combustion processes, the fossil fuel is burnt in an atmosphere of mainly oxygen and recycled CO_2. The flue gas should ideally consist of CO_2 and water vapour only. In practice, there will be a considerable amount of "non-condensable" diluents in the form of oxygen, nitrogen, and argon caused by air leakage, impure oxygen supply from cryogenic air separation, and a certain stoichiometric oxygen surplus in the combustor.

The flue gas typically contains 75–85 mol% CO_2 on a wet basis, and 85–95 mol% after water removal [21,22]. These are highly favourable conditions for low-temperature CO_2 processing units (CPUs), technologies that are considered the most efficient means for removing the volatile components and purifying CO_2. Separation and purification are usually achieved by compressing and partially condensing the flue gas mixture at temperatures down to around −50 °C. Different process layouts of CPUs for CO_2 capture in oxyfuel processes have been proposed [22–27].

2.3. CO_2 Capture in Pre-Combustion Syngas and Hydrogen Production Processes

With high CO_2 fractions in the syngas and syngas separation products, CO_2 separation and purification can be achieved by cooling and partial condensation. The CO_2 fraction, and correspondingly the partial pressure, are highly dependent on the fossil energy source, as well as the reforming/gasification and the hydrogen separation technologies. Oxygen-blown coal gasification can provide pressurised syngas with a sufficiently high CO_2 fraction, allowing for a high CO_2 capture ratio through the direct use of low-temperature CO_2 separation [28–30].

Reforming processes for natural gas generate syngas with CO_2 content typically in the range of 15–25 mol% after the water–gas shift reactions [21]. This range is considerably below what is viable for the partial condensation and separation of liquefied CO_2, but the use of hydrogen-selective separation processes such as pressure-swing adsorption or hydrogen-selective membranes can produce tail gas or retentate gas with highly favourable conditions, with respect to CO_2 fraction [4,31–33].

2.4. Exergy Analysis of Low-Temperature CO_2 Separation Processes

Common key performance indicators (KPIs) found in the literature are related to specific power requirements, the CO_2 capture ratio, CO_2 capture cost, or CO_2 avoidance cost. While the specific power requirement is a useful KPI, it does not provide information about the exergy efficiency of a process and the performance relative to the minimum exergy requirement.

Regarding reported exergy efficiencies of low-temperature CO_2 capture units, another issue requiring careful consideration is the applied definition of exergy efficiency. As one illustrative example, reference [23] presents an oxyfuel CPU that—in the base case—captures 94.11% of the CO_2 from a flue gas containing 82.4 mol% CO_2, with a final CO_2 product purity of 96.9 mol%. The CO_2 product pressure is 18.4 bar while the CO_2-depleted off gas leaves the process at 28.8 bar. The exergy efficiency η is reported to be 67.8%, based on the following definition:

$$\eta = 1 - \frac{E_D + E_L}{E_F} \quad (1)$$

In Equation (1), $E_D + E_L$ equals the total irreversibility rate as the sum of internal exergy destruction (E_D) and external exergy losses (E_L), and E_F is defined as the "total fuel exergy of the system". As discussed and exemplified in previous publications, such as [34], there are different ways to define and assess exergy efficiency from the exergy balance of processes. In [3], it is argued that a rigorous definition of exergy efficiency is the ratio between the minimum exergy requirement, $\dot{E}_{in,min}$, and the actual exergy input to the process, $\dot{E}_{in,act}$:

$$\psi = \frac{\dot{E}_{in,min}}{\dot{E}_{in,act}} \quad (2)$$

From the exergy data of the process streams in [23], the minimum exergy requirement based on the state of the feed and product streams, $\dot{E}_{in,min}$, is 36.93 MW or 63.10 kWh per ton of CO_2 captured. Since the actual exergy input, $\dot{E}_{in,act}$, is 116.16 kWh per ton of CO_2 captured, the resulting exergy efficiency, ψ, becomes 54.3%, which is 13.5% points lower than originally reported.

This numerical example of the exergy efficiency assessment highlights an important issue: While the exergy balance of a process can be rigorously calculated from the mass and energy balance, the chosen model for thermophysical properties, and the defined ambient conditions, the exergy efficiency can be defined and interpreted in several different ways [34]. This implies that when defining exergy efficiency, an element of subjectivity can be present, which in turn can result in different evaluations of the process performance.

3. Method: Exergy Analysis

The concept of exergy provides a tool for revealing the thermodynamic losses and useful output for a given process. With a correct formulation and quantification of the exergy balance with credible and representative thermophysical property models, the exergy balance reveals the useful exergy transfer and the complementary exergy losses, or irreversibilities, for each process unit as well as for the overall process. From the exergy balance, the identification of causal mechanisms (e.g., friction loss, heat loss, mixing loss, etc.) and the location of each irreversibility contribution can in turn be evaluated and ranked with respect to improvement opportunities. Furthermore, exergy is a prerequisite for determining the performance of reversible processes. Depending on the nature of the process, this can be either the minimum exergy requirement for obtaining a desired transformation/conversion of feed(s) into the product(s), or alternatively, the maximum obtainable exergy output, given a set of feed(s) and product(s). Based on this information, the actual performance can be compared to what is theoretically achievable in order to determine the exergy-based efficiency and evaluate the potential for improvement. Dodge [35] formulated this in the following way: "With the reversible process as our standard, we know at once

whether an actual process is already highly efficient or whether it is very inefficient and therefore capable of considerable improvement".

3.1. Exergy Components

In a flowing system, the exergy of a material stream is defined as the maximum work that can be extracted when it is brought from its current state to a dead state, in which it is in equilibrium with the ambient surroundings. The molar exergy ($\bar{e}$) can be expressed as the sum of thermomechanical ($\bar{e}^{\mathrm{tm}}$), chemical ($\bar{e}^{\mathrm{ch}}$), kinetic ($\bar{e}^{\mathrm{kin}}$), and potential ($\bar{e}^{\mathrm{pot}}$) exergies:

$$\bar{e} = \bar{e}^{\mathrm{tm}} + \bar{e}^{\mathrm{ch}} + \bar{e}^{\mathrm{kin}} + \bar{e}^{\mathrm{pot}} \tag{3}$$

The exergy of a process stream can be reduced to the sum of thermomechanical and chemical exergies only, on the assumption that kinetic and potential exergies are of insignificant orders of magnitude in a thermal process. Whereas the kinetic exergy certainly cannot be neglected in the internals of compressors, turbines, and ejectors, the functioning of which is based on the acceleration and deceleration of velocities, the overall kinetic exergy differences between the inlet and outlet can be neglected in most other cases.

The molar thermomechanical exergy of a process stream is expressed in Equation (4), and it is a function of the enthalpies and entropies at the current state ($\bar{h}$, $\bar{s}$) and ambient state ($\bar{h}_0$, $\bar{s}_0$), as well as the ambient temperature (T_0) itself:

$$\bar{e}^{\mathrm{tm}} = \bar{h} - \bar{h}_0 - T_0(\bar{s} - \bar{s}_0) \tag{4}$$

The molar chemical exergy of a mixture can be expressed as follows:

$$\bar{e}^{\mathrm{ch}} = \sum_j x_j \bar{e}_j^{\mathrm{ch}} + \bar{h}_0 - \sum_j x_j \bar{h}_{j,0} - T_0 \left(\bar{s}_0 - \sum_j x_j \bar{s}_{j,0} \right) \tag{5}$$

Here, x_j and $\bar{e}_j^{\mathrm{ch}}$ denote the molar fraction and molar chemical exergy for each single chemical component in the mixture. $\bar{h}_{j,0}$ and $\bar{s}_{j,0}$ denote the respective molar enthalpy and entropy for each single component in pure form at ambient conditions (T_0, p_0).

3.2. Exergy Balance of a Control Volume

Figure 2 illustrates a generic process control volume with m boundary-crossing inlet exergy flows, $\dot{E}_{in}$, and k outlet exergy flows, $\dot{E}_{out}$. Each flow carries exergy in the form of either matter, power, or heat. The total irreversibilities, $\dot{I}_{tot}$, occurring within the boundaries of the control volume can be calculated from the exergy flows crossing the boundaries. The expression for total irreversibility rate in Equation (6) will be referred to as the top-down approach in the following:

$$\dot{I}_{tot} = \sum_{j=1}^{m} \dot{E}_{in,j} - \sum_{j=1}^{k} \dot{E}_{out,j} \tag{6}$$

Inside the control volume, there are n individual elements of irreversibility that are caused by exergy destruction in the various process units or sub-processes. The irreversibility rate, $\dot{I}_j$, for each individual process unit can be calculated from the local exergy balance, applying Equation (6) to the local control volume. The number of individual irreversibility components n in Equation (7) depends on the chosen resolution or abstraction level applied in the subdivision of the process into process elements. If all stand-alone irreversibility rates are added together, the total irreversibility rate can be calculated with what will be referred to as the bottom-up approach:

$$\dot{I}_{tot} = \sum_{j=1}^{n} \dot{I}_j \tag{7}$$

So, it is possible to calculate the overall process irreversibility rate in two independent ways, and it is possible to verify the consistency of irreversibility calculations by comparing these two numbers [36,37]. An element generally lacking in exergy analyses presented in the literature is the checks and balances provided by a transparent comparison of the total irreversibility rate calculated by the top-down and bottom-up expressions, as provided in Equations (6) and (7), respectively.

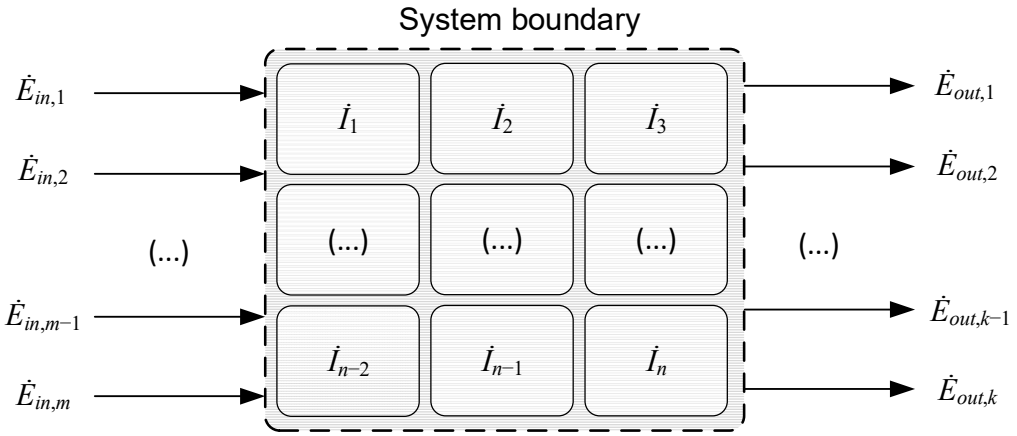

Figure 2. Generic system boundary with m inlet and k outlet exergy flows (material streams, power, and heat) as well as n individual irreversibility components inside the control volume.

The present work will, in detail, analyse the exergy balance and the resulting exergy efficiency of a low-temperature tail gas separation unit for CO_2 capture and the recycling of recovered energy components (methane, CO, and hydrogen) in a hydrogen production plant. All irreversibilities will be allocated and quantified both in a top-down and bottom-up manner, and the results from the two approaches will be compared in a transparent way to verify consistency.

In order to locate and quantify the drivers of irreversibilities in the separation unit, the exergy balance for all individual sub-process units must be established and calculated. The methods for achieving this are described in Section 3.4.

3.3. Minimum Exergy Requirement

Processes such as separation, liquefaction, or compression have defined tasks that involve bringing about a desired change for one or more defined feed streams into one or more product streams. The feed and product streams are in turn defined by properties such as the flow rate, temperature, pressure, and chemical composition. Before considering an actual process layout and assessing its performance, the minimum exergy requirement, $\dot{E}_{in,min}$, can be calculated based on the exergy flows of the defined feed and product streams. A reversible separation process with one feed stream with exergy flow $\dot{E}_{feed}$ and two product streams with exergy flows $\dot{E}_{prod,1}$ and $\dot{E}_{prod,2}$ is used as an illustration in Figure 3. What is also indicated is the inward-directed exergy flow, denoted as $\dot{E}_{in,min}$. Assuming the process is reversible, Equation (6) applied to the control volume reduces to the following:

$$\dot{E}_{in,min} = \dot{E}_{prod,1} + \dot{E}_{prod,2} - \dot{E}_{feed} \quad (8)$$

3.4. Irreversibilities in Process Components

The total irreversibility of a larger process can be obtained from the balance of boundary-crossing exergy flows as expressed in Equation (6), but this figure provides no further information about the location and magnitude of each driver of irreversibilities. As mentioned at the start of Section 3, one of the main purposes of exergy analysis is to identify where and to what extent losses occur in different parts of a system. This in

turn reveals where improvements have the largest potential. A detailed breakdown of irreversibilities will detail each individual term on the right-hand side of Equation (7), which in turn provides information on a much lower level of abstraction than the left-hand side term in Equation (6). Hence, expressions must be established for each defined process element in order to calculate the individual irreversibilities. In the following, the necessary relations for all process units present in the low-temperature tail gas separation process will be developed.

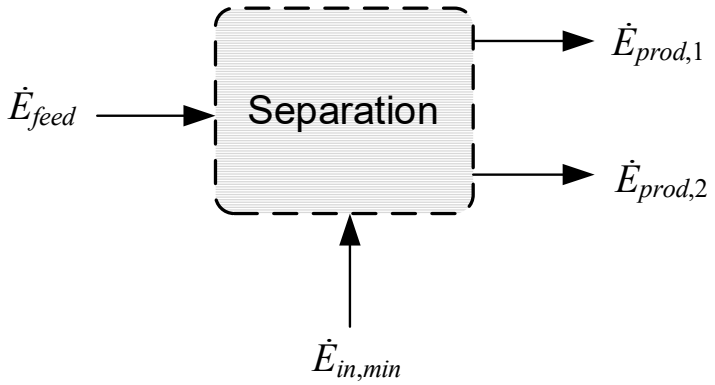

Figure 3. Reversible separation process.

3.4.1. Heat Exchangers

For a well-insulated heat exchanger with n streams, the following expression for the irreversibility rate can be derived by combining Equations (4) and (6):

$$\dot{I}_{HX} = \sum_{j=1}^{n} \dot{m}_j \left[-T_0 \left(s_{in,j} - s_{out,j} \right) \right] \tag{9}$$

Since there are no chemical reactions or mixing of streams, all terms related to chemical exergy in Equation (5) are eliminated from the equation, and the irreversibility rate can, thus, be expressed by the ambient temperature (T_0), specific or molar entropies (s, $\bar{s}$), and mass or molar flow rates ($\dot{m}$, $\dot{N}$) of the process streams.

It is possible to lower the abstraction level further by decomposing $\dot{I}_{HX}$ into irreversibilities caused by heat transfer across finite temperature differences ($\dot{I}^{Q}$) and by pressure losses ($\dot{I}^{\Delta p}$):

$$\dot{I}_{HX} = \dot{I}^{Q} + \dot{I}^{\Delta p} \tag{10}$$

The heat transfer-related irreversibility $\dot{I}^{Q}$ is a function of the ambient temperature, and temperatures on the hot and cold sides of the heat exchanger. It can be calculated from the temperature composite curves of the heat exchanger by the following expression:

$$\dot{I}^{Q} = T_0 \int_0^{\dot{Q}} \frac{\Delta T}{T_H T_C} \delta \dot{Q} \tag{11}$$

Here, T_H and T_C denote the temperatures of the hot and cold composite curves as functions of the heat exchanger duty, $\dot{Q}$, while ΔT is the difference between T_H and T_C. As can be observed, the local heat transfer irreversibility is proportional to the temperature difference, ΔT, but inversely proportional to both T_H and T_C.

Irreversibilities caused by pressure losses, $\dot{I}^{\Delta p}$, are calculated for each individual process stream. The sum of pressure loss-related irreversibilities for a heat exchanger with n process streams can be expressed as follows [37]:

$$\dot{I}^{\Delta p} = \sum_{j=1}^{n} \left[\dot{m}_j T_0 \int_{p_{j,in}}^{p_{j,out}} -\frac{1}{\rho_j T_j} dp_j \right] \tag{12}$$

Here, $\dot{m}_j$ denotes the mass flow rate of stream j, and ρ_j, T_j, and p_j denote the local properties of density, temperature, and pressure for stream j through the heat exchanger pass, respectively.

The two approaches to quantify heat exchanger irreversibilities enable an additional opportunity to verify the results, since the heat exchanger irreversibility obtained from Equation (9) can be checked against the corresponding results obtained from combining Equations (10)–(12). The first approach is quick and simple, but the second approach is more cumbersome and requires two sets of integrals in the domains of heat and pressure in the heat exchanger.

3.4.2. Compressors and Intercoolers

Figure 4 illustrates and defines separate control volumes for an adiabatic compressor with a downstream intercooler. Referring to the indicated stream numbering, the irreversibility rate for the control volume enclosing the compressor can be expressed either as

$$\dot{I}_{cpr} = \dot{W}_{cpr} + \dot{m}(h_1 - h_2 - T_0(s_1 - s_2)), \tag{13}$$

or

$$\dot{I}_{cpr} = \dot{m} T_0 (s_2 - s_1) \tag{14}$$

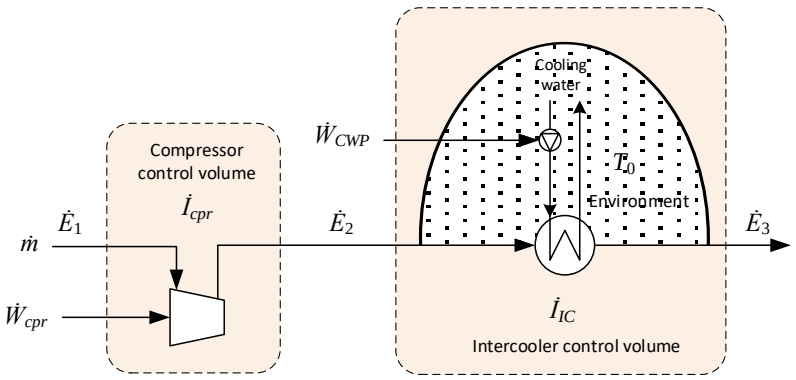

Figure 4. Control volumes for adiabatic compression and subsequent cooling.

The illustrated cooling stage uses water as the heat sink, pressurised by a cooling water pump (CWP) on the cold side. The setup in Figure 4 is also applicable to air-blown intercoolers by replacing the pump symbol and power input with those of an air fan. In the heat exchanger, cooling water is heated, and a certain portion of the thermomechanical exergy is transferred from the compressed gas to cooling water.

By including a portion of the environment in the control volume, the external irreversibilities can be internalised [38]. By doing so, all elements of exergy destruction occurring inside the heat exchanger due to heat transfer and pressure drop, as well as the additional dissipation of pumping power and the rejection of waste heat from the water to

the environment, can be included. In this case, the total irreversibility for the inter-cooling stage can be expressed as follows:

$$\dot{I}_{IC} = \dot{W}_{CWP} + \dot{m}(h_2 - h_3 - T_0(s_2 - s_3)) \quad (15)$$

3.4.3. Expanders

The expander used in the low-temperature tail gas separation process (see Section 4) is not used to recover power, but to induce a temperature drop in the gas stream. In the absence of an electric generator, the expander is coupled to a brake compressor through a shaft in order to transfer and dissipate power. The transferred power is used to compress gas in a closed loop that includes a throttling valve and a cooler located outside the coldbox rejecting heat to the ambient surroundings. As for the intercooler in Figure 4, the control volumes of the expander and brake compressor in Figure 5 also extend into the environment so that all exergy transferred to the brake gas loop is eventually accounted for as irreversibilities. Based on these assumptions and the stream numbering in Figure 5, the irreversibility of the defined control volume can be expressed as follows:

$$\dot{I}_{exp} = \dot{m}(h_1 - h_2 - T_0(s_1 - s_2)) \quad (16)$$

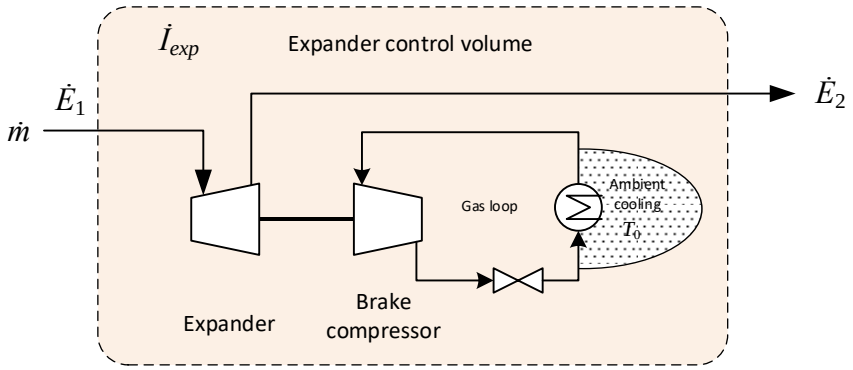

Figure 5. Control volume for the expander and brake compressor.

3.4.4. Regenerative Solid Desiccant Dehydration Unit

The regenerative drying unit consists of one or more parallel active desiccant beds, where water in the inlet gas stream is adsorbed onto the packing material. After a certain amount of time operating in the active mode, the bed is regenerated at a lower pressure and high temperature. In the present case, regeneration is achieved by recycling a relatively small stream of dry gas. The dry gas is throttled to the regeneration pressure and heated before flowing through the bed in the regeneration mode, as illustrated in Figure 6. The recycled gas is then cooled so that water condenses and can be separated and rejected to the environment.

The regeneration process consists of different modes of operation, such as depressurisation, heating, regeneration, cooling, and repressurisation, all with different durations and dependent on the exact design and procedures of the drying process. As one example, the electric heater is active only during the removal of water in the regenerating bed. After the solid desiccant has been regenerated, the recycled gas stream will still be flowing through the regenerating bed, but now with the heater switched off so that the packing material is cooled down before switching to the active mode. A consequence of this is that the flow of rejected water will be present only in certain periods of operation. Due to the batch nature of the regeneration process, the representation of the flow of energy and matter is provided in time-averaged terms. Using average values, the exergy balance for the control volume in Figure 6 can be expressed as follows:

$$\dot{I}_{dry} = \dot{E}_1 + \dot{W}_{CWP} + \dot{W}_{el} + \dot{E}_{REC,in} - \left(\dot{E}_2 + \dot{E}_{REC,out}\right) \quad (17)$$

Similar to the ambient cooler in Figure 4, a portion of the environment is included in the control volume of the cooler in Figure 6. The condensed water is assumed to be rejected to the environment so that the exergy of the water stream is accounted for as an element of irreversibility in the control volume.

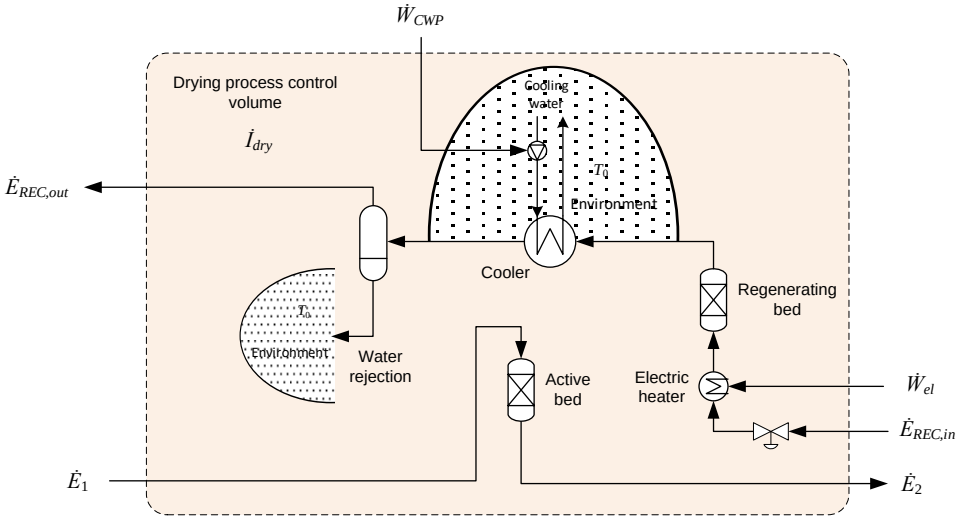

Figure 6. Control volume for the regenerative solid desiccant drying unit.

3.4.5. Other Components: Mixers, Separators, and Valves

The mixing of streams can cause irreversibilities caused by differences in composition, pressure, and temperature. For an adiabatic mixer, the resulting irreversibility rate can be calculated by combining Equations (4)–(6), where all exergy flows in and out of the mixing point correspond to material streams.

The same equations apply to separators, provided that they are assumed to be well-insulated and, therefore, adiabatic. In the case of an adiabatic vapour–liquid separator with a single inlet stream, this will result in zero irreversibilities (neglecting kinetic and potential exergy terms, as discussed in Section 3.1). In the case of multiple inlets, an adiabatic separator may cause irreversibilities due to the mixing effects. Irreversibilities in a vapour–liquid separator at sub-ambient temperature can also be caused by heat leakage from the ambient surroundings, the significance of which is further discussed in a sensitivity analysis in Section 5.6.

For an adiabatic and isenthalpic throttling valve, the following expression for irreversibility can be derived from Equations (4) and (6):

$$\dot{I}_{valve} = \dot{m} T_0 (s_2 - s_1) \tag{18}$$

4. Process Description

4.1. Hydrogen Production Plant with CO_2 Capture

The tail gas separation cycle in consideration is part of a hydrogen production process with integrated CO_2 capture and a capacity of 500 tons of hydrogen per day, as previously documented in [4]. A process flow diagram is given in Figure 7. The core technology of the reforming plant is an oxygen-blown autothermal reforming (ATR) section for syngas generation. A pre-reformer first converts higher hydrocarbons in the natural gas feed to methane, before the feed is further heated and mixed with a fraction of the CO_2-depleted tail gas recycled from the gas separation section, and then sent to the main reformer. The tail gas recycling to the ATR reactor represents a difference from the process documented in [4], where tail gas is recycled only to the water–gas shift section. After cooling in a steam generation section, the syngas passes through a high- and low-temperature water–gas shift reactor (HT-WGS and LT-WGS, respectively) to increase the carbon monoxide to CO_2 conversion, and correspondingly, the hydrogen production. A second fraction of

the CO_2-depleted tail gas is recycled to the LT-WGS reactor to increase the overall carbon monoxide conversion. Although all reactors correspond to types found in conventional plants, the recycling of tail gas from the gas separation to the ATR and LT-WGS reactors represents a novelty that can enable the simultaneous achievement of very high efficiency, decarbonisation ratio, and hydrogen recovery ratio [4].

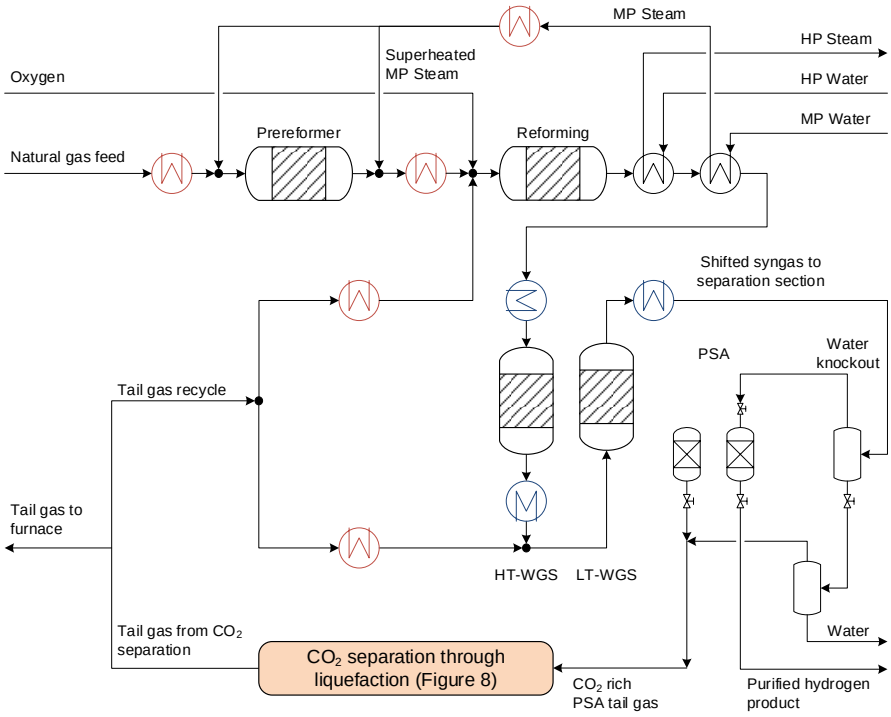

Figure 7. Process flow diagram for the hydrogen production process based on an autothermal reformer, two water–gas shift reactors, and a PSA unit for hydrogen separation and purification. The sub-process "CO_2 separation through liquefaction" is explained in detail in Section 4.2. Coolers are represented in blue while heaters are shown in red. The reader is referred to the web version for the colour coding.

After the water–gas shift reactors, the shifted syngas is cooled to a near ambient temperature before the condensed water, with a certain amount of dissolved gas components, is removed by phase separation. The condensed water is subsequently flashed to recover a fraction of the dissolved CO_2. After water knockout, the syngas is separated into high-purity hydrogen retained at high pressure and tail gas discharged at low pressure using a conventional PSA. Although this process consists of parallel batch units (see Section 4.2 for further discussion about stability and continuity), it is modelled as a continuous black-box unit with the following main assumptions, which are considered conservative:

- 1.1 bar(a) tail gas discharge pressure;
- 85% hydrogen recovery ratio.

Upon discharge, the low-pressure, CO_2-rich PSA tail gas is mixed with the gas stream from the condensed water flash unit and passed on to the low-temperature tail gas separation unit.

The hydrogen production process is modelled as a steady-state process in Aspen HYSYS 10.0 using the cubical Peng–Robinson equation of state to calculate thermophysical fluid properties. All reactors are modelled as equilibrium reactors. The surplus heat of the process is utilised in a steam cycle. The steam cycle includes high, medium, and low-pressure stages for power generation. All heaters and coolers in Figure 7, as well as the heaters in the steam cycle, are included for a subsequent pinch analysis. The pinch analysis is achieved through a coupled Python script that automatically extracts the required values from the HYSYS simulation. An in-depth description of the process, as well as a detailed

analysis of the process, can be found in Straus et al. [4]. Table 1 shows the chosen process conditions and the corresponding KPIs. These differ slightly from those provided in Straus et al. [4]: CO_2-depleted tail gas is also recycled here to the ATR in addition to the LT-WGS, and the total fraction of recycled tail gas is slightly increased as it enables higher overall efficiency of the process. Another modification is that the hydrogen recovery in the PSA is reduced and is, therefore, specified more conservatively in this work.

Table 1. Summary of the chosen parameters and key performance indicators, adjusted from Straus et al. [4].

Parameter/KPI	Unit	Value
Tail gas recycle	%	93
Fraction of tail gas recycled to ATR	%	25
$T_{Feed,LT\text{-}WGS}$	°C	200
Carbon capture rate	%	98.24
Higher heating value efficiency	%	84.44
Lower heating value efficiency	%	78.34

4.2. Low-Temperature Unit for CO_2 Capture and Tail Gas Recovery and Recycling

A process flow diagram for the low-temperature unit with stream numbering is shown in Figure 8. The main sections of the process are:

- Multi-stage tail gas compression with intercoolers and dehydration unit;
- Heat exchanger network for partial condensation of the compressed tail gas;
- Main separation vessel for phase separation of the partially condensed tail gas;
- Three-stage flash separation for CO_2 purification and flash gas recycling to compressors;
- Auxiliary cascade refrigeration cycle with propane and ethane as refrigerants;
- Pressurisation of the purified CO_2 by liquid pumping.

Disclosure of data for process streams, compressors, heat exchangers, and more is provided in tabular form in Appendix A.

Although the PSA unit is a batch process with respect to pressurisation, blowdown, and purge, configurations with parallel columns cycling between the different operation modes can provide a (close-to) continuous flow of separation products. The low-pressure tail gas discharged from the PSA is assumed to be supplied with a constant chemical composition and at otherwise steady-state conditions. This should be a reasonable assumption based on practical experience from PSA tail gas compression, where, respectively, 1–2% and 0.2–0.4% volume flow fluctuations at the compressor suction and discharge are reported [39]. In addition to the buffering capabilities in the compression section, the vapour–liquid separators in the process will provide additional buffering capacity so that a steady flow of separation products can be provided.

The tail gas is compressed in five inter-cooled stages, from a 1.1-bar suction pressure to a 56.5-bar discharge pressure. At the suction of the three last stages, the tail gas stream is mixed with gas streams from the three flash separation stages. While the tail gas feed has a CO_2 fraction of 60.9 mol%, the first two flash gas recycle streams have significantly higher CO_2 fractions, which leads to an enrichment of CO_2. The final recycle stream has a CO_2 fraction marginally below that of the feed stream, and the resulting CO_2 fraction of the stream entering the coldbox is about 63.5 mol%. Intercoolers in the tail gas compressor train reduce the gas temperature to 23 °C by cooling water, with a specific power requirement in the water pumps equivalent to 0.007 MJ_p per MJ_{th} rejected heat.

Between the fourth and fifth compression stages, the tail gas undergoes deep dehydration in a molsieve desiccant bed. As mentioned in Section 3.4.4, while the drying process in the active bed is continuous, the overall drying unit operates as a batch process in the depressurisation, regeneration, cooling, and repressurisation stages of the desiccant bed operation. It is operated with parallel beds in active mode or regeneration mode to ensure continuous dehydration. The active bed continuously dehydrates the tail gas at an inlet

pressure of 32.7 bar with a pressure drop of 1 bar from the inlet to the outlet; the pressure level of the regenerated bed is 18 bar. Regeneration heat is provided by electricity for heating a smaller flow of dry tail gas (REC01), equivalent to 6% of the total flow rate of the dehydrated stream. The dry regeneration gas is extracted downstream of the dehydration unit. Due to the batch nature of the regeneration cycle, the specific power requirement of the regeneration cycle is given as an average value of 8 MJ per kg of water removed. This figure includes the duty of the electric heater as well as cooling water pumping for condensing out water from the recycle stream.

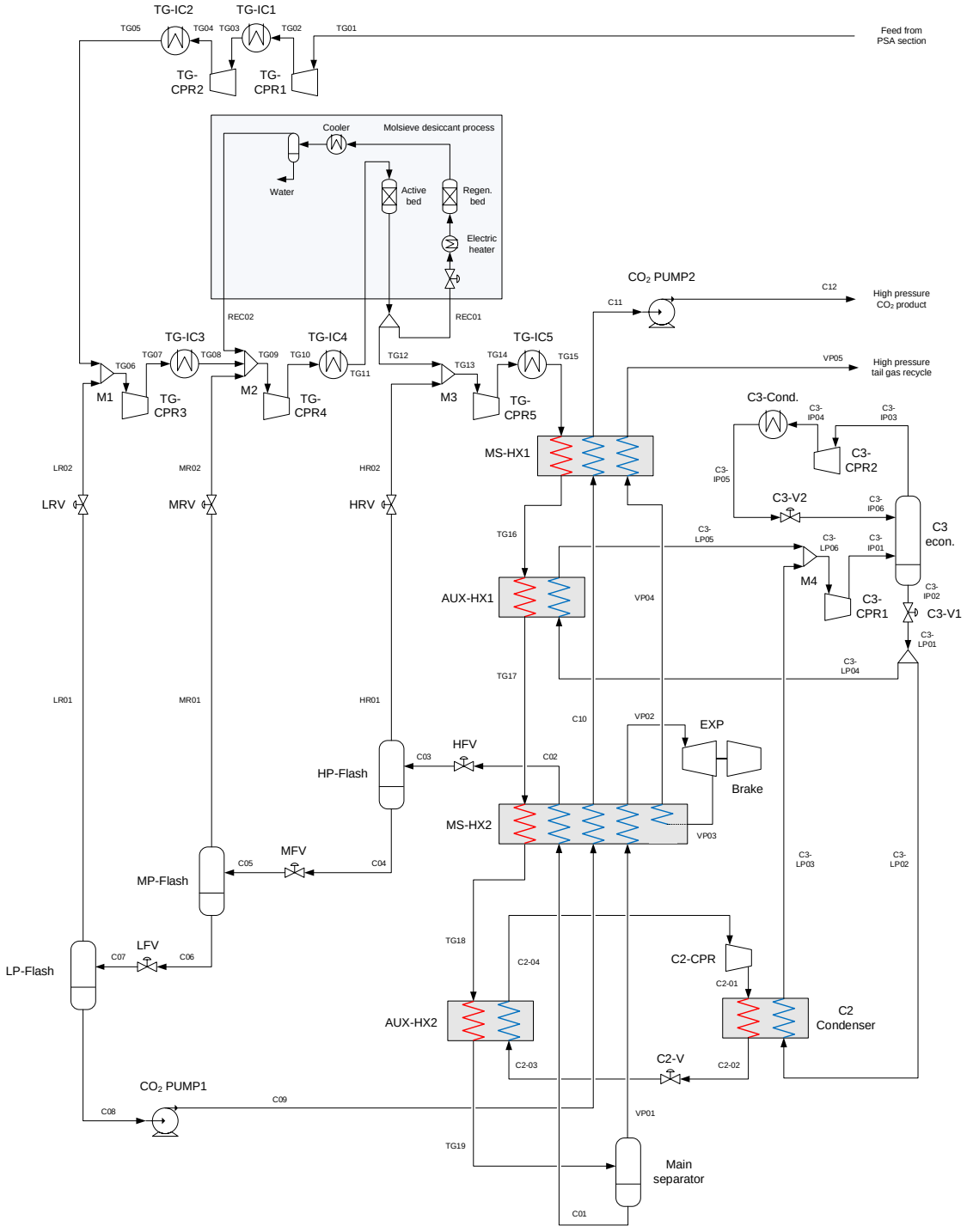

Figure 8. Process flow diagram for the low-temperature tail gas separation and CO_2 capture unit. Also included is the auxiliary refrigeration cycle with propane and ethane as refrigerants in a cascade cycle.

It should be mentioned that given the availability of high-temperature heat in the heat recovery section of the hydrogen production plant, and the possibility of partial integration with intercooler heat, more rational means for heat supply are possible from the viewpoint of thermodynamic efficiency. To avoid excessive integration measures, electric power for heating is assumed in the current process, thereby incurring some additional thermodynamic losses compared to what could be achieved with heat integration.

After compression and dehydration, the pressurised tail gas is cooled to −53 °C in a network of heat exchangers inside an insulated coldbox. Two multi-stream plate–fin heat exchangers (MS-HX1, MS-HX2) ensure heat integration between the feed stream and the process streams while the remainder of the refrigeration duty is provided by two heat exchangers transferring heat to the auxiliary propane and ethane refrigeration cycles (AUX-HX1, AUX-HX2). Figure 9 shows the temperature composite curves for the four heat exchangers. Minimum temperature approach constraints are set to 3 °C for MS-HX1, MS-HX2, and AUX-HX1, and 2 °C in the cold end of AUX-HX2, where the temperature is relatively close to the freeze-out temperature for CO_2. As discussed in [30], and based on [40], −53 °C/−55 °C on the tail gas/refrigerant sides in the cold end of AUX-HX2 is unlikely to pose any risk of CO_2 freeze-out, and even lower separator temperatures may be applicable.

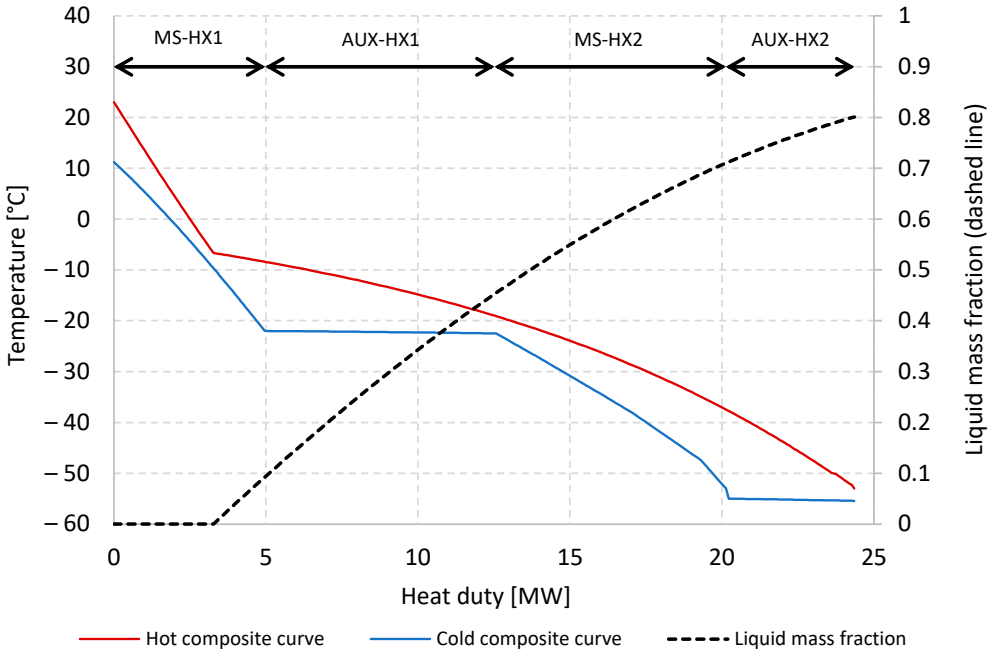

Figure 9. Temperature composite curves and liquid mass fraction for the four heat exchangers used to cool and partially condense the tail gas stream.

At the main separator inlet, the liquid mass fraction in the partially condensed tail gas stream is around 0.80, with 90.1% of the CO_2 liquefied. The liquid-phase CO_2 fraction is 95.6 mol% with the complementary fraction (4.4 mol%) consisting of dissolved hydrogen, methane, CO, and nitrogen. In the main separator, the CO_2-rich liquid phase is separated from the CO_2-depleted vapour phase, which has a hydrogen fraction of 53.9 mol%. The liquid stream is subsequently stripped of the volatile components in a three-stage flash separation cascade to obtain higher CO_2 purity. To avoid freeze-out as well as to enhance the purification of CO_2, the high-pressure liquid stream is heated to −22.5 °C in MS-HX2 before flashing. The pressure level of each flash stage is matched with the suction pressure of compressors TG-CPR3–5, adjusted with a 0.1-bar pressure loss in each recycle stream. Pressure levels in the flash separators are 31.80 bar, 17.10 bar, and 6.94 bar. At the liquid outlet of the final flash stage, the temperature is −50.7 °C, and a CO_2 purity of 99.85 mol% is achieved. In order to reach the 110-bar target pressure for the purified CO_2 product, the

liquid stream is pumped in two stages; initially to 70 bar to limit the required pressure rating of the heat exchangers (MS-HX1 and MS-HX2), and finally to 110 bar after heating.

As described in Section 4.1, the vapour product from the main separator is, to a high degree, recycled to reactors in the hydrogen production plant along with a smaller fraction for purge and thermal recuperation via a combustor. To maximise the heat recuperation of the vapour product, it is first used to cool the tail gas feed stream in MS-HX1 and MS-HX2. Since there is a potential to also utilise parts of the pressure-based exergy of this stream, it is expanded from 54.7 bar to 42.3 bar in a low-temperature turbine. The expansion induces a 15.5 °C temperature drop, which enables the re-use of the stream in a second cold-side pass in MS-HX2, thereby increasing the recuperation and further reducing the required duty of auxiliary refrigeration. The shaft power of the turbine is assumed to be dissipated by a turbine brake connected to the same shaft, as described in Section 3.4.3.

The auxiliary refrigeration cycle is designed to provide evaporative refrigeration duty on the cold side of heat exchangers (AUX-HX1 and AUX-HX2) to compensate for the deficit in refrigeration duty. The propane cycle has two compressor stages raising the pressure between the evaporator pressure at 2.27 bar, with intermediate pressure at 3.46 bar and the high-pressure level for condensation at 9.50 bar. In the condenser, propane is cooled by water to 23 °C, giving it a slight subcooling before the stream is throttled into the economiser at the intermediate pressure stage. The liquid stream extracted from the economiser is throttled down to the evaporator pressure and distributed to heat exchangers AUX-HX1, providing refrigeration for tail gas cooling, and the cascade C2 condenser for ethane condensation. The process for distributing propane to these heat exchangers can be configured with different layouts, for instance, by locating the splitter immediately downstream of the liquid outlet, and with two individual throttling valves replacing C3-V1 in Figure 8. This would enable the distribution of the two propane refrigerant streams in the liquid phase. This avoids the need for splitting a two-phase stream, which may easily lead to maldistribution. However, for the purpose of the present work, the choice of configuration will not affect mass and energy balances, the exergy balance, or other results since AUX-HX1 and the C2 condenser have equal evaporation pressures.

5. Results and Discussion

The energy supplied to the low-temperature tail gas separation process is entirely made up of power. The main portion (about 82%) of the power input is caused by the need for tail gas compression. A summary of the power requirements is given in Table 2, while a more detailed breakdown of compressor power is provided in Appendix A.

Table 2. Summary of power requirements.

	Power [kW]	**Specific Power [MJ/ton CO_2 Captured]**	**Percentage of Total**
Tail gas compression	28,059.7	579.6	82.0%
Auxiliary refrigeration	4418.4	91.3	12.9%
Molsieve regeneration	767.9	15.9	2.2%
Liquid CO_2 pumping	650.6	13.4	1.9%
Cooling water pumping	326.7	6.7	1.0%
Total power requirement	34,223.3	706.9	100%

The power requirement in the tail gas separation unit equals 34.22 MW (or 706.9 MJ/ton CO_2, in specific terms). This states the amount of power required per mass unit of CO_2 captured at high purity and high pressure but does not reveal the actual efficiency of the process. In order to determine the exergy efficiency as expressed in Equation (2), the minimum exergy requirement must be calculated.

Furthermore, in order to understand the causes and drivers of exergy losses and to pinpoint potential ways to improve efficiency, an exergy analysis of all sub-process

units is required. In the following, a detailed exergy analysis will be presented, with the following purposes:

- To derive the minimum exergy requirement for transforming the tail gas feed stream into the specified separation products;
- To calculate the exergy efficiency of this process;
- To provide full transparency of the causes of exergy losses,

providing the following:

- A detailed explanation of the required power input to the process;
- Transparent checks and balances to verify that all irreversibilities are accounted for by disclosing the relative difference in the independent irreversibility calculations based on the bottom-up and top-down approaches (see Equations (6) and (7));
- A basis for assessing further opportunities for improving the process efficiency.

5.1. Minimum Exergy Requirement for the Tail Gas Separation Unit

The minimum exergy requirement is obtained from Equations (3)–(5) and (8), and equals the difference between the exergy flows of the two product streams, C12 and VP05, and the feed stream, TG01. Process stream properties are provided in Appendix A, while the calculated exergy flows are presented graphically and numerically in Figure 10.

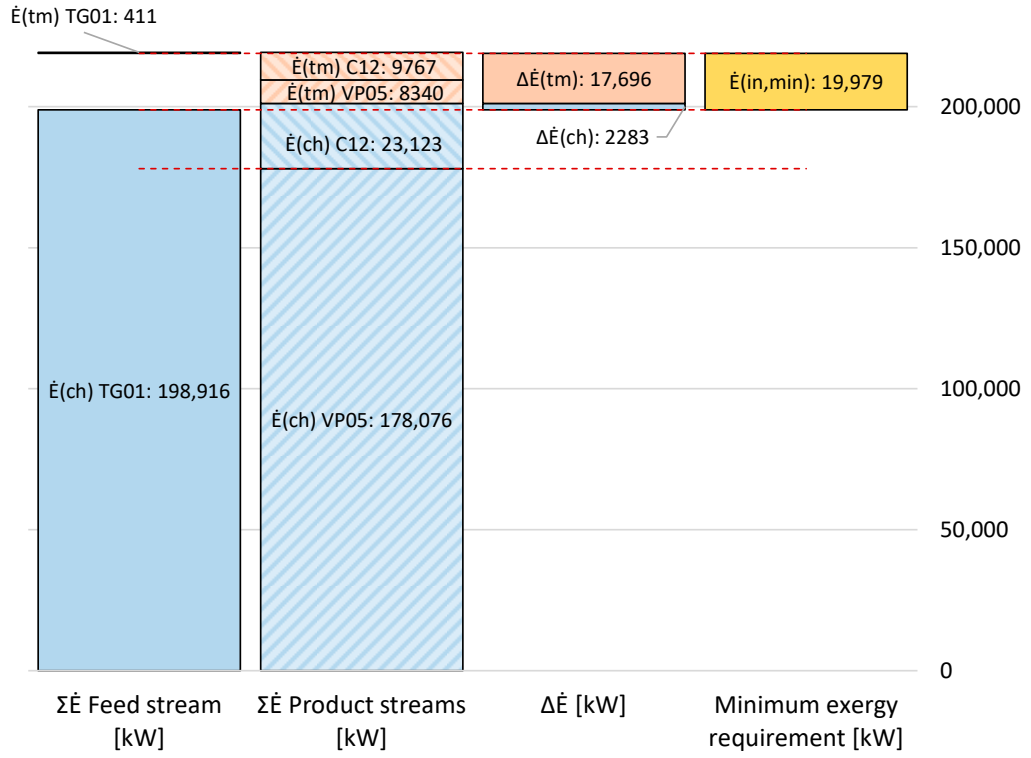

Figure 10. Thermomechanical (tm) and chemical (ch) exergy flows of the feed stream, TG01, and product streams, C12 and VP05. The difference in exergy flow equals the minimum exergy requirement for the tail gas separation process.

As can be observed, the exergy transfer and, thus, the minimum exergy input to the process amounts to 19,979 kW. Of this, the main exergy transfer consists of an increase in thermomechanical exergy, equal to 17,696 kW, while the corresponding increase in chemical exergy equals 2283 kW. In specific terms, the minimum exergy requirement scaled by the flow rate of captured CO_2 is 412.7 MJ/ton$_{CO2}$. However, it should be mentioned that for this particular process, both separation products are key outputs. Therefore, scaling the exergy requirement with the flow rate of CO_2 and using it as a key performance indicator is associated with a degree of ambiguity. As can be observed in Figure 10, almost half of

the thermomechanical exergy is transferred to the process stream, VP05, 93% of which is recycled to the hydrogen plant (see Table 1). So, the task of the tail gas separation process is to provide a high-pressure, high-purity CO_2 product, and a recyclable, high-pressure, CO_2-depleted tail gas stream.

5.2. Distribution of Process Irreversibilities

By applying the methodology to quantify the individual irreversibilities described in Section 3.4, exergy losses are calculated for 42 different process units or components, comprising a total of 50 irreversibility elements. The results are summarised in Figure 11 and broken down into two different stacked bar diagrams.

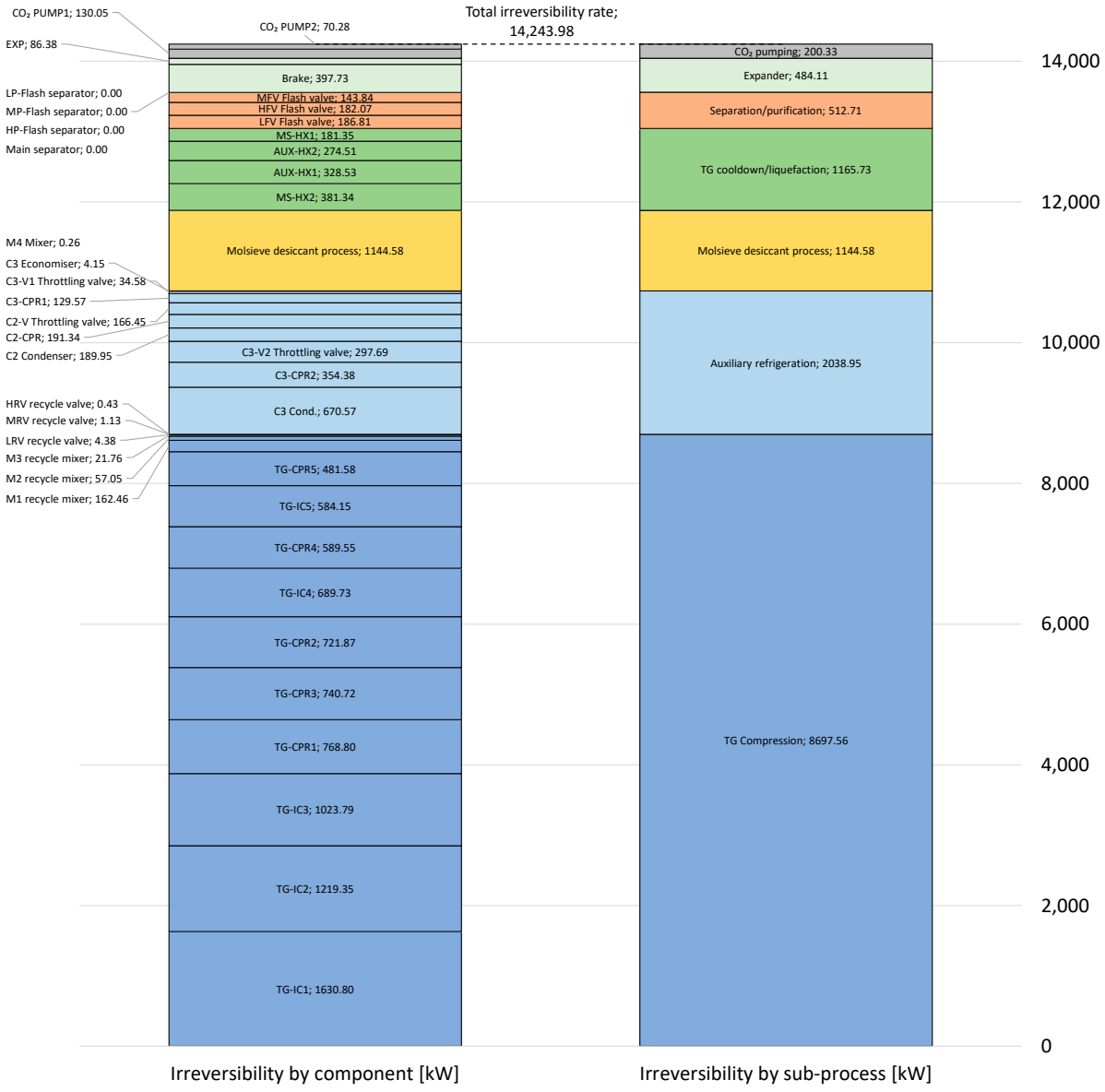

Figure 11. Total irreversibility rate divided into process units (left-hand side) and grouped into sub-processes (right-hand side). Colours are used to differentiate between sub-processes.

The left-hand stack shows the contribution from each of the 42 components, while the right-hand stack shows results for 7 different sub-processes. As shown in Table 2, tail gas compression is by far the dominant driver for power input to the process. This is also the case with respect to irreversibilities in the system, where the tail gas compressors and intercoolers account for around 61.1% of the total irreversibilities. Auxiliary refrigeration

is second to tail gas compression with respect to irreversibilities and causes around 14.3% of the total irreversibilities. The desiccant dehydration process causes around 8.0% of the total irreversibilities, and the sum of losses in the four heat exchangers, MS-HX1, MS-HX2, AUX-HX1, and AUX-HX2, is of a similar magnitude, around 8.2%.

As can be observed from the decomposed irreversibility numbers, the separation and purification units, which comprise the main separator and three flash stages, account for only about 513 kW, or only 3.6% of the overall losses. These losses are entirely caused by the throttling valves upstream of each flash separation stage. The irreversibility rate in each separator equals zero since each separator itself is assumed to be adiabatic, at phase equilibrium, and otherwise has no inlet or outlet losses due to the neglection of kinetic and potential exergy terms. The C3 economiser in the auxiliary refrigeration cycle, to which the same assumptions apply, and is attributed to an irreversibility rate of about 4 kW. This is explained by the fact that this separator has two inlet streams with different temperatures, which in turn causes irreversibilities caused by mixing effects in the vessel. The significance of heat leakage into the low-temperature separation vessels is discussed in the sensitivity analysis in Section 5.6.

5.3. Irreversibility Components in Process Heat Exchangers

Heat exchangers contribute to a significant portion of overall irreversibilities. While the five compressor intercoolers cause a total irreversibility of 5148 kW, mainly due to the complete dissipation of waste heat, the four low-temperature heat exchangers for partial liquefaction of the tail gas cause a total irreversibility of 1166 kW. Although the total irreversibility incurred in each heat exchanger can be determined by Equation (9) from the entropy and flow rate of each inlet and outlet process stream, Equations (11) and (12) make it possible to determine the separate irreversibility components caused by heat transfer and pressure drop.

Figure 12 shows the temperature composite curves and cumulative irreversibility components for the coldbox heat exchangers, MS-HX1, MS-HX2, AUX-HX1, and AUX-HX2. In each diagram, the cumulate values for $\dot{I}^{Q}$ and $\dot{I}^{\Delta p}$ are plotted as functions of the normalised heat transfer with the cold end of the heat exchanger as the reference point. It should be noted that the text on the two vertical axes (left and right) applies to all four diagrams. In all heat exchangers, the heat transfer across finite temperature differences is the dominant cause of irreversibility. MS-HX1 is the unit with the highest share of irreversibility caused by the pressure drop, corresponding to 22.7% of the irreversibility. In MS-HX2, the corresponding percentage is 12.4%, while roughly 9% of irreversibilities are caused by the pressure drop in heat exchangers AUX-HX1 and AUX-HX2.

5.4. Consistency of Irreversibility Calculations

To corroborate the numerical results of the exergy analysis and verify the consistency of the exergy balance, the two independent calculations for irreversibilities given by Equations (6) and (7) should be compared. Discrepancies between the two numbers will imply potential errors in the exergy calculations and bookkeeping methodology, but without locating or pinpointing such discrepancies.

Table 3 presents the total irreversibility rate quantified by the independent top-down and bottom-up approaches, where the first figure is based on boundary-crossing exergy flows and the second equals the sum of 50 individual irreversibility terms for 42 different components (see Figure 11). As can be observed, the relative difference between the two numbers is $4 \cdot 10^{-7}$, which is of an order of magnitude reflecting the background accuracy of convergence in the simulation software. The consistency between the top-down and the detailed bottom-up irreversibility calculations is, therefore, considered verified.

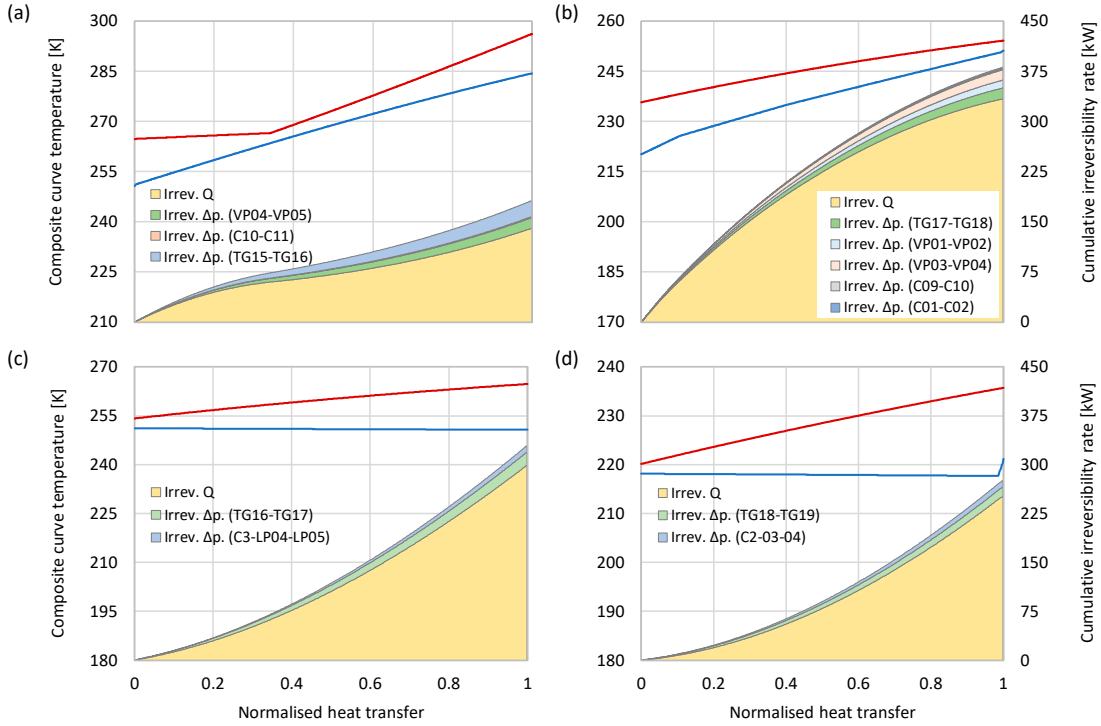

Figure 12. Temperature composite curves (red and blue lines) and irreversibilities in the heat exchanger, (**a**) MSHX-1, (**b**) MSHX-2, (**c**) AUX-HX1, and (**d**) AUX-HX2. Irreversibilities are decomposed into exergy destruction caused by heat transfer (Irrev. Q) and pressure drop (Irrev. Δp).

Table 3. Comparison of irreversibility results from top-down and bottom-up methods.

	Top-Down Calculation, Equation (6)	Bottom-Up Calculation, Equation (7)	Relative Difference
Irreversibility [kW]	14,243.970	14,243.975	$4{\cdot}10^{-7}$

5.5. Exergy Efficiency

Equation (2) defines the exergy efficiency of the low-temperature tail gas separation process as the ratio between the minimum theoretical work and actual work for transforming the feed stream into the two separation products at desired thermodynamic states. The minimum exergy requirement for this process is calculated to be 19,979 kW, as given in Figure 10, while the corresponding power requirement in the current process configuration is found to be 34,223 kW, as given in Table 2. Thus, the resulting exergy efficiency becomes 58.38%.

This result may be checked against a more general definition of exergy efficiency, such as the rational efficiency [38],

$$\psi = \frac{\sum_{i=I}^{m} \Delta \dot{E}_{out,i}}{\sum_{i=I}^{n} \Delta \dot{E}_{in,i}} \tag{19}$$

where each numerator term represents useful exergy output, and each denominator term represents necessary exergy input. In the separation process in consideration, there is no main product and by-product, but rather two useful products, as discussed in Section 5.1. The useful output of the process can, thus, be considered as the sum of increased chemical exergy and increased thermomechanical exergy, while the necessary input equals the sum of power consumption:

$$\psi = \frac{\Delta \dot{E}^{\mathrm{ch}} + \Delta \dot{E}^{\mathrm{tm}}}{\sum_{i=I}^{n} \dot{W}_i} \tag{20}$$

When comparing the third and fourth columns in Figure 10, it becomes clear that the sum of increased chemical and thermomechanical exergies equals the minimum exergy requirement for the process. Therefore, the numerical values of the numerator and denominator are equal in the two expressions for exergy efficiency given by Equations (2) and (20), thus giving the same result.

5.6. Sensitivity Analysis

The exergy balance and resulting exergy efficiency of the low-temperature tail gas separation unit rely on an extensive set of assumptions that are summarised in Appendix A. To supplement the baseline results that are used as a basis to derive the exergy balance and efficiency figures, a supplementary sensitivity analysis is presented in Table 4. A selection of variables is subject to arbitrary changes, and the stand-alone impact each change has on the total irreversibility rate, power requirement, and exergy efficiency is ranked in descending order.

Table 4. Summary of sensitivity analysis.

Sensitivity Variable	Variable Change	Irreversibilities [kW]	Power Requirement [kW]	Exergy Efficiency	Consistency of Exergy Balance Convergence [1]
Compressor efficiencies [%]	−5% points	16,320	36,299	55.04%	$9{\cdot}10^{-10}$
HX pressure losses	+100%	15,766	35,713	55.85%	$2{\cdot}10^{-7}$
HX minimum ΔT [°C]	+2 °C	14,830	34,809	57.40%	$1{\cdot}10^{-6}$
Ambient coolers outlet T [°C]	+7 °C	14,664	34,651	57.68%	$6{\cdot}10^{-7}$
Dehydration, recycle ratio	+4% points	14,460	34,439	58.01%	$2{\cdot}10^{-7}$
Separator heat leakage [W]	+1000 W [2]	14,247	34,226	58.37%	$2{\cdot}10^{-7}$
Baseline results	—	14,244	34,223	58.38%	$4{\cdot}10^{-7}$

[1] Relative deviation in total irreversibility calculated by Equations (6) and (7). [2] Into each separator.

Since the compression of the tail gas and the refrigerants makes up about 95% of the total exergy input, it is obvious that the overall efficiency is sensitive to compressor efficiencies. A 5% point reduction in each compressor's isentropic efficiency reduces the overall exergy efficiency by 3.3% points. Second to this sensitivity, it was found that doubling pressure losses in all heat exchangers and ambient coolers in the process reduces the exergy efficiency by 2.5% points.

In the baseline results, all separators and the refrigeration cycle economiser are considered adiabatic. Even with two insulating barriers (surface insulation and cold-box insulation), there will be a certain heat leakage from the ambient surroundings. Given the size of the plant and vapour–liquid separators, the potential heat leakage is assumed to be in the kilowatt order of magnitude. Hence, the aggregate impact of 1000 W of heat leakage into each vessel was evaluated and was found to reduce the exergy efficiency by only 0.01% points.

6. Discussion

It should be emphasised that the variable changes in Table 4 represent stricter assumptions that result in higher irreversibilities and power demand, and consequently, lower exergy efficiency. Thus, no upside potentials with respect to efficiency are presented here, although obvious opportunities for improvements exist. As an example, the recovery of the expander power in the form of mechanical or electric power has the potential to improve the exergy efficiency by up to around 0.7% points. Another possibility for power recovery is to compress the vapour product stream (VP05) with a compressor drawing power directly from the expander shaft before the CO_2-depleted vapour product is recycled to the hydrogen production plant. This will allow a higher pressure ratio across the expander and, thus, a higher induced temperature drop, which in turn will increase the internal heat

recuperation and correspondingly reduce the duty of AUX-HX2 as well as the compressor duties in the auxiliary refrigeration cycles.

Turbines can theoretically replace the throttling valves HFV, MFV, and LFV in the CO_2 purification section. It should be noted that these valves have a combined irreversibility of 512.7 kW, which is considerable in proportion when compared to, for instance, the multi-megawatt low-temperature heat exchangers. As one example, the LFV valve has an irreversibility rate of about 182 kW, which is virtually equal to the total irreversibilities in MS-HX1, which has a thermal duty close to 5 MW. Replacing the throttling valves with expanders would theoretically reduce the entropy production and, thus, the irreversibilities associated with CO_2 purification. However, the applicability of such expanders must be investigated in depth, as the freeze-out of the cold CO_2-rich liquid due to pressure- and enthalpy drops in nozzles and impellers cannot be ruled out. Moreover, such expanders must be able to handle a two-phase outlet flow.

Ambient coolers in the tail gas compression section and the auxiliary refrigeration cycle account for almost 41% of the total process irreversibilities. Hence, it is obvious that the utilisation of waste heat has—at least theoretically—the potential to improve the overall exergy efficiency. The highest temperatures of rejected heat are found after the first and second compressor stages, with discharge temperatures of 116.9 °C and 110.7 °C, respectively. Perhaps the most obvious potential for internal recuperation of waste heat is found in the molsieve desiccant dehydration process, which is the only section of the process with a heat demand above ambient temperature. Therefore, the power requirement and, thus, irreversibilities in the dehydration process can theoretically be reduced by a partial heat integration with the cooling of compressed tail gas. Depending on the plant's co-location with adjacent industries, the external utilisation of waste heat can also be envisaged.

7. Conclusions

In order to estimate the exergy efficiency of the tail gas separation unit and to quantify and locate the cause of thermodynamic losses in the form of irreversibilities, a detailed exergy analysis was conducted for a proposed configuration of the tail gas processing cycle as part of a large-scale 500 t/d hydrogen production plant.

The total irreversibility rate is made up of 42 identified components and 7 sub-processes. The main portion of exergy demand, 82%, is caused by the need for tail gas compression. This is also reflected in the exergy balance, where 61.1% of irreversibilities are caused by tail gas compression and inter-cooling. The other drivers for irreversibilities are found to be auxiliary refrigeration (14.3%), solid desiccant dehydration (8.0%), coldbox heat exchangers for tail gas cooling and liquefaction (8.2%), CO_2 separation/purification (3.6%), the cold expander and expander brake system (3.4%), and CO_2 pumps (1.4%).

Two independent calculations for the total irreversibility rate in the low-temperature separation units were performed to check the degree of consistency and thereby verify the results obtained from the exergy analysis. Comparing the sum of individual irreversibilities in all 42 different components with the corresponding irreversibility rate obtained from the balance of exergy flows crossing the system boundaries, it is concluded that the two methods yield identical results, as the relative difference between the independent calculations is $4 \cdot 10^{-7}$. Given the current set of assumptions applied to the process model, the overall exergy efficiency and the rational efficiency of the low-temperature tail gas separation process are both calculated to be 58.38%.

A supplementary sensitivity analysis suggests that the main uncertainty with respect to exergy efficiency pertains to the efficiency of compressors used for tail gas compression and auxiliary refrigerant compression. This is explained by the fact that about 95% of the exergy requirement is supplied as compressor power, which in turn affects irreversibilities in compressors as well as intercoolers.

Author Contributions: Conceptualization, D.B., J.S. and T.G.; methodology, D.B., J.S. and T.G.; validation, D.B.; formal analysis, D.B.; writing—original draft preparation, D.B. and J.S.; writing—review and editing, T.G.; visualization, D.B. and J.S.; supervision, T.G. All authors have read and agreed to the published version of the manuscript.

Funding: This research was funded by the Research Council of Norway (Norges forskningsråd).

Data Availability Statement: The original contributions presented in the study are included in the article and Appendix A. Further inquiries can be directed to the corresponding author.

Acknowledgments: The authors acknowledge the Research Council of Norway for basic funding supporting this work.

Conflicts of Interest: D.B. and J.S. are inventors of the one granted Norwegian patent no. 347086, titled "Method for production of H2 with high carbon capture ratio and efficiency", and on a patent-pending application "Method for production of h2 with high carbon capture ratio and efficiency" (EP4263424A1; PCT/NO2021/050264); they are co-inventors on a patent-pending application, "Method and plant for separation of carbon dioxide (co2)" (PCT/EP2023/065703). The funders had no role in the design of the study; in the collection, analyses, or interpretation of data; in the writing of the manuscript; or in the decision to publish the results.

Nomenclature

E_D	exergy destruction
E_F	"fuel exergy"
E_L	exergy loss
$\dot{E}$	exergy flow rate
$\dot{E}_{in,min}$	minimum exergy requirement
$\dot{E}_{in,act}$	actual exergy input
$\bar{e}$	molar exergy
h	specific enthalpy
$\bar{h}$	molar enthalpy
$\dot{I}$	irreversibility rate
$\dot{m}$	mass flow rate
$\dot{N}$	molar flow rate
p	pressure
$\dot{Q}$	heat rate
s	specific entropy
$\bar{s}$	molar entropy
T	temperature
$\dot{W}$	power, rate of work
x	molar fraction
Greek symbols	
η	efficiency
Δ	difference
ρ	mass density
ψ	exergy efficiency, rational efficiency
Subscripts	
0	ambient
C	cold
cpr	compressor, compression
CWP	cooling water pump
dry	drying, dehydration
el	electric
exp	expander, expansion
H	hot
HX	heat exchanger
IC	intercooler

j	integer counter
p	power
prod	product
REC	recycle
th	thermal
tot	total
Superscripts	
ch	chemical
kin	kinetic
pot	potential
Q	heat transfer
tm	thermomechanical
Δp	pressure loss

Appendix A

Table A1. Process stream data.

Stream ID	Temperature	Pressure	Molar Flow	Enthalpy	Entropy	Chemical Composition [mol%]							
	°C	bar	kmol/h	kJ/kmol	kJ/(kmol-K)	CH_4	CO_2	N_2	CO	H_2O	H_2	C_3H_8	C_2H_6
C01	−53.00	55.00	5049.9	−395,822	78.15	1.09	95.61	1.65	0.63	0.00	1.02	—	—
C02	−22.50	54.70	5049.9	−393,152	89.49	1.09	95.61	1.65	0.63	0.00	1.02	—	—
C03	−25.43	31.80	5049.9	−393,152	89.95	1.09	95.61	1.65	0.63	0.00	1.02	—	—
C04	−25.43	31.80	4802.7	−400,800	87.71	0.84	97.51	0.97	0.38	0.00	0.30	—	—
C05	−32.87	17.10	4802.7	−400,800	88.08	0.84	97.51	0.97	0.38	0.00	0.30	—	—
C06	−32.87	17.10	4463.6	−407,318	84.00	0.45	99.06	0.32	0.13	0.00	0.03	—	—
C07	−50.72	6.94	4463.6	−407,318	84.52	0.45	99.06	0.32	0.13	0.00	0.03	—	—
C08	−50.72	6.94	3966.0	−411,740	76.72	0.10	99.85	0.03	0.01	0.00	0.00	—	—
C09	−47.46	70.00	3966.0	−411,419	77.13	0.10	99.85	0.03	0.01	0.00	0.00	—	—
C10	−22.00	69.70	3966.0	−409,219	86.36	0.10	99.85	0.03	0.01	0.00	0.00	—	—
C11	11.21	69.40	3966.0	−405,634	99.72	0.10	99.85	0.03	0.01	0.00	0.00	—	—
C12	16.56	110.00	3966.0	−405,365	99.94	0.10	99.85	0.03	0.01	0.00	0.00	—	—
HR01	−25.43	31.80	247.2	−244,539	133.45	6.06	58.70	14.75	5.48	0.00	15.01	—	—
HR02	−25.51	31.70	247.2	−244,539	133.47	6.06	58.70	14.75	5.48	0.00	15.01	—	—
LR01	−50.72	6.94	497.6	−372,078	146.72	3.24	92.75	2.64	1.07	0.00	0.30	—	—
LR02	−50.90	6.84	497.6	−372,078	146.83	3.24	92.75	2.64	1.07	0.00	0.30	—	—
MR01	−32.87	17.10	339.1	−315,003	141.79	5.89	77.11	9.51	3.64	0.00	3.85	—	—
MR02	−33.01	17.00	339.1	−315,003	141.83	5.89	77.11	9.51	3.64	0.00	3.85	—	—
REC01	23.00	31.70	522.6	−256,736	137.15	2.60	63.68	8.35	2.91	0.00	22.45	—	—
REC02	23.00	17.00	522.6	−256,387	143.17	2.60	63.68	8.35	2.91	0.00	22.45	—	—
TG01	23.00	1.10	7369.3	−245,773	165.91	2.40	60.93	8.66	2.99	0.26	24.75	—	—
TG02	116.93	3.05	7369.3	−242,442	167.22	2.40	60.93	8.66	2.99	0.26	24.75	—	—
TG03	23.00	2.75	7369.3	−245,809	158.21	2.40	60.93	8.66	2.99	0.26	24.75	—	—
TG04	110.65	7.14	7369.3	−242,727	159.44	2.40	60.93	8.66	2.99	0.26	24.75	—	—
TG05	23.00	6.84	7369.3	−245,896	150.42	2.40	60.93	8.66	2.99	0.26	24.75	—	—
TG06	17.87	6.84	7866.9	−253,878	150.45	2.46	62.94	8.28	2.87	0.24	23.20	—	—
TG07	101.80	17.30	7866.9	−250,982	151.63	2.46	62.94	8.28	2.87	0.24	23.20	—	—
TG08	23.00	17.00	7866.9	−253,944	142.90	2.46	62.94	8.28	2.87	0.24	23.20	—	—
TG09	20.68	17.00	8728.6	−256,462	142.96	2.60	63.54	8.33	2.91	0.22	22.41	—	—
TG10	79.87	33.00	8728.6	−254,496	143.80	2.60	63.54	8.33	2.91	0.22	22.41	—	—
TG11	23.00	32.70	8728.6	−256,769	136.84	2.60	63.54	8.33	2.91	0.22	22.41	—	—
TG12	23.00	31.70	8186.8	−256,736	137.15	2.60	63.68	8.35	2.91	0.00	22.45	—	—
TG13	21.54	31.70	8434.0	−256,378	137.07	2.70	63.53	8.54	2.99	0.00	22.24	—	—
TG14	74.00	56.50	8434.0	−254,741	137.78	2.70	63.53	8.54	2.99	0.00	22.24	—	—
TG15	23.00	56.20	8434.0	−256,928	131.00	2.70	63.53	8.54	2.99	0.00	22.24	—	—
TG16	−8.40	55.90	8434.0	−259,051	123.33	2.70	63.53	8.54	2.99	0.00	22.24	—	—
TG17	−19.00	55.60	8434.0	−262,272	110.96	2.70	63.53	8.54	2.99	0.00	22.24	—	—
TG18	−37.44	55.30	8434.0	−265,519	97.77	2.70	63.53	8.54	2.99	0.00	22.24	—	—
TG19	−53.00	55.00	8434.0	−267,322	89.89	2.70	63.53	8.54	2.99	0.00	22.24	—	—
VP01	−53.00	55.00	3384.1	−75,570	107.41	5.11	15.67	18.83	6.50	0.00	53.89	—	—
VP02	−22.50	54.70	3384.1	−74,546	111.81	5.11	15.67	18.83	6.50	0.00	53.89	—	—
VP03	−38.03	42.31	3384.1	−74,969	112.13	5.11	15.67	18.83	6.50	0.00	53.89	—	—

Table A1. *Cont.*

Stream ID	Temperature	Pressure	Molar Flow	Enthalpy	Entropy	Chemical Composition [mol%]							
	°C	bar	kmol/h	kJ/kmol	kJ/(kmol-K)	CH_4	CO_2	N_2	CO	H_2O	H_2	C_3H_8	C_2H_6
VP04	−22.50	42.01	3384.1	−74,462	114.28	5.11	15.67	18.83	6.50	0.00	53.89	—	—
VP05	11.21	41.70	3384.1	−73,374	118.41	5.11	15.67	18.83	6.50	0.00	53.89	—	—
C3-LP01	−22.00	2.27	2796.1	−124,068	76.46	—	—	—	—	—	—	100	—
C3-LP02	−22.00	2.27	1150.6	−124,068	76.46	—	—	—	—	—	—	100	—
C3-LP03	−19.49	2.23	1150.6	−107,355	143.14	—	—	—	—	—	—	100	—
C3-LP04	−22.00	2.27	1645.5	−124,068	76.46	—	—	—	—	—	—	100	—
C3-LP05	−22.49	2.23	1645.5	−107,559	142.33	—	—	—	—	—	—	100	—
C3-LP06	−21.25	2.23	2796.1	−107,475	142.67	—	—	—	—	—	—	100	—
C3-IP01	−3.82	3.46	2796.1	−106,440	143.25	—	—	—	—	—	—	100	—
C3-IP02	−9.87	3.46	2796.1	−124,068	76.30	—	—	—	—	—	—	100	—
C3-IP03	−9.87	3.46	3675.6	−106,873	141.62	—	—	—	—	—	—	100	—
C3-IP04	33.21	9.50	3675.6	−104,430	142.82	—	—	—	—	—	—	100	—
C3-IP05	23.00	9.20	3675.6	−120,284	89.67	—	—	—	—	—	—	100	—
C3-IP06	−9.88	3.46	3675.6	−120,284	90.68	—	—	—	—	—	—	100	—
C2-01	17.04	15.50	1488.5	−86,207	168.83	—	—	—	—	—	—	—	100
C2-02	−18.71	15.20	1488.5	−99,126	118.88	—	—	—	—	—	—	—	100
C2-03	−55.00	4.60	1488.5	−99,126	120.28	—	—	—	—	—	—	—	100
C2-04	−52.00	4.52	1488.5	−88,913	167.22	—	—	—	—	—	—	—	100

Table A2. Efficiencies and power of compressors, pumps, and the expander.

	Isentropic Efficiency	Polytropic Efficiency	Shaft Power
	%	%	kW
Tail gas compressor, stage 1	85.0	86.6	6819.9
Tail gas compressor, stage 2	85.0	86.5	6307.8
Tail gas compressor, stage 3	85.0	86.5	6329.7
Tail gas compressor, stage 4	85.0	86.1	4765.9
Tail gas compressor, stage 5	85.0	86.0	3836.4
Propane compressor, stage 1	85.0	85.4	804.4
Propane compressor, stage 2	85.0	86.0	2495.3
Ethane compressor	83.0	84.9	1118.8
Expander	85.0	84.5	397.7
LT CO_2 pump	75.0		353.6
HT CO_2 pump	75.0		297.0

Table A3. Heat exchanger data.

Heat Exchanger ID	Minimum Temperature Approach	Pressure Drop per Pass	Thermal Duty
	°C	kPa	kW
MS-HX1	3.0	30	4972.3
AUX-HX1	3.0	4–30	7546.2
MS-HX2	3.0	30	7608.5
AUX-HX2	2.0	8–30	4222.6
C2 Condenser	3.3	4–30	5341.5

Table A4. Other assumptions.

Dehydration, specific power	$MJ_p/kg\ H_2O$	8
Molsieve bed, pressure drop	kPa	100
Molsieve regeneration recycle ratio	%	6
Ambient coolers, outlet temperature	°C	23
Ambient coolers, pressure drop	kPa	30
Ambient coolers, specific pumping power	MJ_p/MJ_{th}	0.007

References

1. Seck, G.S.; Hache, E.; Sabathier, J.; Guedes, F.; Reigstad, G.A.; Straus, J.; Wolfgang, O.; Ouassou, J.A.; Askeland, M.; Hjorth, I.; et al. Hydrogen and the decarbonization of the energy system in europe in 2050: A detailed model-based analysis. *Renew. Sustain. Energy Rev.* **2022**, *167*, 112779. [CrossRef]
2. Pruvost, F.; Cloete, S.; del Pozo, C.A.; Zaabout, A. Blue, green, and turquoise pathways for minimizing hydrogen production costs from steam methane reforming with CO_2 capture. *Energy Convers. Manag.* **2022**, *274*, 116458. [CrossRef]
3. Berstad, D.; Gundersen, T. On the exergy efficiency of CO_2 capture: The relation between sub-process and overall efficiencies. *Carbon Capture Sci. Technol.* **2023**, *7*, 100111. [CrossRef]
4. Straus, J.; Skjervold, V.T.; Anantharaman, R.; Berstad, D. Novel approach for low CO_2 intensity hydrogen production from natural gas. *Sustain. Energy Fuels* **2022**, *6*, 4948–4961. [CrossRef]
5. Tuinier, M.; Annaland, M.v.S.; Kuipers, J. A novel process for cryogenic CO_2 capture using dynamically operated packed beds—An experimental and numerical study. *Int. J. Greenh. Gas Control* **2011**, *5*, 694–701. [CrossRef]
6. Tuinier, M.; Hamers, H.; Annaland, M.v.S. Techno-Economic evaluation of cryogenic CO_2 capture—A comparison with absorption and membrane technology. *Int. J. Greenh. Gas Control* **2011**, *5*, 1559–1565. [CrossRef]
7. Clodic, D.; Hitti, R.; Younes, M.; Bill, A.; Casier, F. CO_2 Capture by Anti-Sublimation Thermo-Economic Process Evaluation. In Proceedings of the Fourth Annual Conference Carbon Capture Sequestration, Alexandria, VA, USA, 2–5 May 2005; pp. 1–11.
8. Clodic, D.; Younes, M.; Bill, A. Test Results of CO_2 Capture by Anti-Sublimation Capture Efficiency and Energy Consumption for Boiler Plants. In *Greenhouse Gas Control Technologies*; Elsevier Science Ltd.: Amsterdam, The Netherlands, 2005; pp. 1775–1780. ISBN 978-0-08-044704-9.
9. Clodic, D.; Younes, M.; Riachi, Y.; El Hitti, R.; Boulawz Ksayer, E.; Pan, X.; Yu, Y. CO_2 Capture by Anti-Sublimation Using Integrated Cascade System. Available online: https://iifiir.org/en/fridoc/co2-capture-by-anti-sublimation-using-integrated-cascade-system-27838 (accessed on 16 January 2024).
10. Tuinier, M.; Annaland, M.v.S.; Kramer, G.; Kuipers, J. Cryogenic CO_2 capture using dynamically operated packed beds. *Chem. Eng. Sci.* **2010**, *65*, 114–119. [CrossRef]
11. Cann, D.; Font-Palma, C.; Willson, P. Moving packed beds for cryogenic CO_2 capture: Analysis of packing material and bed precooling. *Carbon Capture Sci. Technol.* **2021**, *1*, 100017. [CrossRef]
12. Cann, D.; Font-Palma, C.; Willson, P. Experimental analysis of CO_2 frost front behaviour in moving packed beds for cryogenic CO_2 capture. *Int. J. Greenh. Gas Control* **2021**, *107*, 103291. [CrossRef]
13. Jensen, M.J.; Russell, C.S.; Bergeson, D.; Hoeger, C.D.; Frankman, D.J.; Bence, C.S.; Baxter, L.L. Prediction and validation of external cooling loop cryogenic carbon capture (CCC-ECL) for full-scale coal-fired power plant retrofit. *Int. J. Greenh. Gas Control* **2015**, *42*, 200–212. [CrossRef]
14. De, D.K.; Oduniyi, I.A.; Sam, A.A. A novel cryogenic technology for low-cost carbon capture from NGCC power plants for climate change mitigation. *Therm. Sci. Eng. Prog.* **2022**, *36*, 101495. [CrossRef]
15. Babar, M.; Mukhtar, A.; Mubashir, M.; Saqib, S.; Ullah, S.; Quddusi, A.H.A.; Bustam, M.A.; Show, P.L. Development of a novel switched packed bed process for cryogenic CO_2 capture from natural gas. *Process. Saf. Environ. Prot.* **2021**, *147*, 878–887. [CrossRef]
16. Song, C.; Liu, Q.; Ji, N.; Deng, S.; Zhao, J.; Li, Y.; Kitamura, Y. Reducing the energy consumption of membrane-cryogenic hybrid CO_2 capture by process optimization. *Energy* **2017**, *124*, 29–39. [CrossRef]
17. Bouma, R.; Vercauteren, F.; van Os, P.; Goetheer, E.; Berstad, D.; Anantharaman, R. Membrane-assisted CO_2 Liquefaction: Performance Modelling of CO_2 Capture from Flue Gas in Cement Production. *Energy Procedia* **2017**, *114*, 72–80. [CrossRef]
18. Anantharaman, R.; Berstad, D.; Roussanaly, S. Techno-Economic Performance of a Hybrid Membrane—Liquefaction Process for Post-combustion CO_2 Capture. *Energy Procedia* **2014**, *61*, 1244–1247. [CrossRef]
19. Song, C.; Fan, Z.; Li, R.; Liu, Q.; Sun, Y.; Kitamura, Y. Intensification of CO_2 separation performance via cryogenic and membrane hybrid process—Comparison of polyimide and polysulfone hollow fiber membrane. *Chem. Eng. Process.-Process. Intensif.* **2018**, *133*, 83–89. [CrossRef]
20. Li, R.; Lian, S.; Zhang, Z.; Deng, S.; Song, C. Simulation of a novel hybrid membrane-cryogenic process for post-combustion carbon capture. *Carbon Capture Sci. Technol.* **2022**, *5*, 100075. [CrossRef]
21. Berstad, D.; Anantharaman, R.; Nekså, P. Low-temperature CO_2 capture technologies—Applications and potential. *Int. J. Refrig.* **2013**, *36*, 1403–1416. [CrossRef]
22. Magli, F.; Spinelli, M.; Fantini, M.; Romano, M.C.; Gatti, M. Techno-Economic optimization and off-design analysis of CO_2 purification units for cement plants with oxyfuel-based CO_2 capture. *Int. J. Greenh. Gas Control* **2022**, *115*, 103591. [CrossRef]
23. Jin, B.; Zhao, H.; Zheng, C. Optimization and control for CO_2 compression and purification unit in oxy-combustion power plants. *Energy* **2015**, *83*, 416–430. [CrossRef]
24. White, V.; Wright, A.; Tappe, S.; Yan, J. The Air Products Vattenfall Oxyfuel CO_2 Compression and Purification Pilot Plant at Schwarze Pumpe. *Energy Procedia* **2013**, *37*, 1490–1499. [CrossRef]
25. Font-Palma, C.; Errey, O.; Corden, C.; Chalmers, H.; Lucquiaud, M.; del Rio, M.S.; Jackson, S.; Medcalf, D.; Livesey, B.; Gibbins, J.; et al. Integrated oxyfuel power plant with improved CO_2 separation and compression technology for EOR application. *Process. Saf. Environ. Prot.* **2016**, *103*, 455–465. [CrossRef]

26. Kim, S.-I.; Lee, H.; Lee, Y.W.; Yang, W. Performance evaluation of a pressurized oxy-combustion power plant according to wet and dry flue gas recirculation. *Int. J. Greenh. Gas Control* **2021**, *107*, 103277. [CrossRef]
27. van der Spek, M.; Eldrup, N.H.; Skagestad, R.; Ramirez, A. Techno-Economic Performance of State-of-the-Art Oxyfuel Technology for Low-CO_2 Coal-fired Electricity Production. *Energy Procedia* **2017**, *114*, 6432–6439. [CrossRef]
28. Consonni, S.; Viganò, F.; Kreutz, T.; De Lorenzo, L. CO_2 Capture in IGCC Plants via Cryogenic Separation. In Proceedings of the Sixth Annual Conference on Carbon Capture & Sequestration, Pittsburgh, PA, USA, 7–10 May 2007; pp. 7–10.
29. Berstad, D.; Anantharaman, R.; Nekså, P. Low-temperature CCS from an IGCC Power Plant and Comparison with Physical Solvents. *Energy Procedia* **2013**, *37*, 2204–2211. [CrossRef]
30. Berstad, D.; Skaugen, G.; Roussanaly, S.; Anantharaman, R.; Nekså, P.; Jordal, K.; Trædal, S.; Gundersen, T. CO_2 Capture from IGCC by Low-Temperature Synthesis Gas Separation. *Energies* **2022**, *15*, 515. [CrossRef]
31. Kim, D.; Berstad, D.; Anantharaman, R.; Straus, J.; Peters, T.A.; Gundersen, T. Low Temperature Applications for CO_2 Capture in Hydrogen Production. In *Computer Aided Chemical Engineering*; Pierucci, S., Manenti, F., Bozzano, G.L., Manca, D., Eds.; Elsevier: Amsterdam, The Netherlands, 2020; Volume 48, pp. 445–450.
32. Kim, D.; Liu, Z.; Anantharaman, R.; Riboldi, L.; Odsæter, L.; Berstad, D.; Peters, T.A.; Polfus, J.M.; Malerød-Fjeld, H.; Gundersen, T. Design of a Novel Hybrid Process for Membrane Assisted Clean Hydrogen Production with CO_2 Capture through Liquefaction. In *Computer Aided Chemical Engineering*; Yamashita, Y., Kano, M., Eds.; Elsevier: Amsterdam, The Netherlands, 2022; Volume 49, pp. 127–132.
33. Leclerc, M.; Rodrigues, G.; Dubettier, R.; Ruban, S. Optimized configuration to reduce H_2 carbon footprint in a refinery. *Int. J. Greenh. Gas Control* **2022**, *118*, 103671. [CrossRef]
34. Marmolejo-Correa, D.; Gundersen, T. A comparison of exergy efficiency definitions with focus on low temperature processes. *Energy* **2012**, *44*, 477–489. [CrossRef]
35. Dodge, B.F. *Chemical Engineering Thermodynamics*; Chemical Engineering Series; McGraw-Hill Book Company: New York, NY, USA, 1944.
36. Gjennestad, M.A.; Aursand, E.; Magnanelli, E.; Pharoah, J. Performance analysis of heat and energy recovery ventilators using exergy analysis and nonequilibrium thermodynamics. *Energy Build.* **2018**, *170*, 195–205. [CrossRef]
37. Berstad, D.; Skaugen, G.; Wilhelmsen, Ø. Dissecting the exergy balance of a hydrogen liquefier: Analysis of a scaled-up claude hydrogen liquefier with mixed refrigerant pre-cooling. *Int. J. Hydrogen Energy* **2020**, *46*, 8014–8029. [CrossRef]
38. Kotas, T.J. *The Exergy Method of Thermal Plant Analysis*; Krieger Publishing: Malabar, FL, USA, 1995; ISBN 978-0-89464-946-2.
39. Pichot, D.; Granados, L.; Morel, T.; Schuller, A.; Dubettier, R.; Lockwood, F. Start-up of Port-Jérôme CRYOCAP™ Plant: Optimized Cryogenic CO_2 Capture from H_2 Plants. *Energy Procedia* **2017**, *114*, 2682–2689. [CrossRef]
40. Fandiño, O.; Trusler, J.M.; Vega-Maza, D. Phase behavior of (CO_2 + H_2) and (CO_2 + N_2) at temperatures between (218.15 and 303.15) K at pressures up to 15 MPa. *Int. J. Greenh. Gas Control* **2015**, *36*, 78–92. [CrossRef]